Hemicellulose-*g*-PAAc/TiO$_2$ Nanocomposite Hydrogel for Dye Removal

Yudan Li[1], Xiao-Feng Sun[1,2,3,*], Jiayi Chen[1,3] and Le Sun[1]

[1]School of Chemistry and Chemical Engineering, Northwestern Polytechnical University, Xian 710072, China

[2]Research & Development Institute of Northwestern Polytechnical University in Shenzhen, Shenzhen, 518063, China

[3]Dongguan Sanhang Military Civilian Integration Innovation Research Institute, Dongguan, 523808, China

Abstract: Dyes pollution on urban environment is of great concern because of the human health hazards associated with this kind of contaminants, and the use of low-cost photocatalytic composite material is an efficient treatment method to minimize the environmental impact. A novel hemicellulose-*g*-PAAc/TiO$_2$ composite hydrogel was prepared as a promising alternative material for dye removal. Wheat straw hemicellulose and TiO$_2$ nanoparticles were first modified and then incorporated into hydrogel via covalent bonds. Effects of gel dosage, pH, initial concentration and contact time on the adsorption amount of methylene blue were systematically studied using the prepared hydrogel. The equilibrium adsorption data was fitted well to the Freundlich isotherm model, and Langmuir isotherm analysis indicated that the adsorption capacity of the hemicellulose-*g*-PAAc/TiO$_2$ composite hydrogel was 389.1 mg/g, and adsorption kinetic study showed that the adsorption process can be described by the pseudo second-order kinetic model. The prepared composite hydrogel exhibited high photodegradation ability for methylene blue under alkaline conditions, and all results indicated that the hemicellulose-*g*-PAAc/TiO$_2$ composite hydrogel had excellent photocatalytic degradability for dyes, which can be used in practical process.

Keywords: Hemicellulose, nanocomposite hydrogel, adsorption, photocatalytic degradation.

1. INTRODUCTION

With the development of global industrialization process, wastewater pollution especially the dye wastewater which has colors, great toxicity and complex components, is one of the major environmental problems which influence human survival and development. Adsorption is the one common technique for dye wastewater treatment. However, it merely transfers dyes from the liquid to the solid phase causing secondary pollution and requiring further treatment [1]. Photocatalytic degradation is a friendly environmentally technique, which can be conveniently applied to dye pollutants for their degradation.

Hemicellulose is an important polysaccharide in the plant cell wall, which is second only to cellulose. It is one of the three major components of plant biomass, and it is a natural renewable resource to be developed and utilized, compared with cellulose and starch, Hemicellulose has a complex molecular structure, consisting of xylose, arabinose, mannose, glucose, galactose, glucuronic acid, and a small amount of rhamnose and fucose [2]. The main chain of xylan-type hemicellulose is generally composed of D-xylose linked by β-1,4 glycosidic bond and contains various side chains and functional groups [3]. Because of its special molecular structure, hemicellulose has good biocompatibility, biodegradability and anti-cancer efficacy [4-5], and its hydrophilicity is better than cellulose and chitosan. Therefore, the preparation of hydrogel materials from hemicellulose has broad application prospects, especially in environmental treatment, tissue engineering materials and drug release [6,7].

Nanocomposite hydrogel is a kind of nanocomposite material formed by dispersing nanoparticles into hydrogel, and nanoparticles mainly rely on their surface properties or unsaturated bonds to participate in the network structure during the formation of gel, which increases the cross-linking density, thus greatly improving the strength and elasticity of gel. Because nanocomposite hydrogels not only have the unique water absorption characteristics of hydrogels and the functions of nanomaterials themselves, but also have the characteristics of high mechanical strength, strong toughness, excellent thermal stability, easy recovery, etc., and they show broad application prospects in the fields of controlled drug release, catalysts, sensors, environmental engineering, etc. [8-11]. It is found that the composite hydrogel synthesized by adding inorganic particles such as montmorillonite

*Address correspondence to this author at the Research & Development Institute of Northwestern Polytechnical University in Shenzhen, Shenzhen, 518063, China; E-mail: xf001sn@nwpu.edu.cn

[12], bentonite [13], carbon nanotubes [14] into the hydrogel, especially the nanocomposite hydrogel, has a significant effect on improving its performance. At present, our research group is committed to the research of hemicellulose-based organic-inorganic composite hydrogel, and has prepared hemicellulose/carbon nanotube composite hydrogel [15], hemicellulose/Fe_3O_4 composite hydrogel [16] and chemically-crosslinked xylan/graphene oxide composite hydrogel [17].

In this paper, hemicellulose-g-PAAc/TiO_2 composite hydrogel was prepared to remove dye from aqueous solution via adsorption and photocatalytic degradation process. The effects of adsorbent dosage, pH, initial concentration and contact time were investigated.

2. MATERIALS AND METHODS

2.1. Materials

Hemicellulose was isolated from wheat straw according to our previous method [2]. Acrylic acid (AAc) and maleic anhydride were purchased from Tianjin Kermel Chemical Reagent Company in China. The cross-linker N, N-methylenebiacrylamide (Bis) was purchased from Tianjin Hongyan Chemical Reagent Factory in China. Ammonium persulfate and sodium sulfite anhydrous were obtained from Tianjin Fuchen Chemical Reagent Factory in China. Dimethylformamide (DMF), lithium chloride (LiCl) and 4-dimethyaminopyridine were supplied by from J&K Chemical LTD. TiO_2 nanoparticles with a diameter of 30 nm were purchased from Shanghai ST-Nano Science & Technology Co., Ltd. All other reagents used were of analytical grade.

2.2. Synthesis of Hemicellulose Derivatives (HC-MA)

1.00 g of dry hemicellulose material was dissolved in 20 mL distilled water, and then 10 mL of DMF was added, stirring for 5 min. The water was removed from the mixture by evaporation under reduced pressure at 50 °C. DMF/LiCl were found be served as good solvent for hemicelluloses and DMAP is a stronger nucleophile as a catalyst for modification of hemicellulose. In this study, 0.10 g LiCl, 15 mL DMF, and 0.05g of the catalyst DMAP were added, and the temperature was kept at 80 °C. 10 minutes later, 2.97 g maleic anhydride, previously dissolved in 10 mL DMF, was added. The homogeneous reaction mixture was stirred for 8h (Figure **1**). After the reaction, the mixture was cooled to room temperature and slowly poured into 120 mL of ethanol with stirring. The resulting precipitate was washed thoroughly with ethanol and acetone to eliminate any color impurities and by-products. Finally, the product was dried to constant weight for further use.

2.3. Modification of TiO_2 Nanoparticles

Modification of TiO_2 nanoparticles followed the previous method about the modification of Fe_3O_4 [16]. 1g TiO_2 nanoparticles were dispersed in 30 mL of ethanol solution (90%, v/v) under ultrasonic vibration for 15 min. 0.7g of ammonia (25 wt%) and 0.62g silane A151 were then added to this solution, and ammonia was used to regulate the acidity and alkalinity of the solution, and the solution was treated under ultrasonic irradiation for 1 h and then mechanically stirred (500 r/min) for 48h at room temperature (Figure **2**). After the reaction, the solution was filtered and washed repeatedly by ethanol to remove A151 adsorbed on the surface. Finally, the powder (denoted as A151-TiO_2) was dried at 60 °C overnight under vacuum.

2.4. Preparation of Hydrogel

The hydrogel was prepared by free radical polymerization (Figure **3**). 0.5g of HC-MA was fully dissolved in distilled water (10mL) in a beaker with a magnetic stirrer. 0.18g of A151-TiO_2 was dispersed in the solution mentioned above. Subsequently, the redox initiator $(NH_4)_2S_2O_8$-Na_2SO_3 (0.03 g) was added into the solution. After 5 minutes, 1.0g of AAc and the cross-linker Bis were added into the mixed solution.
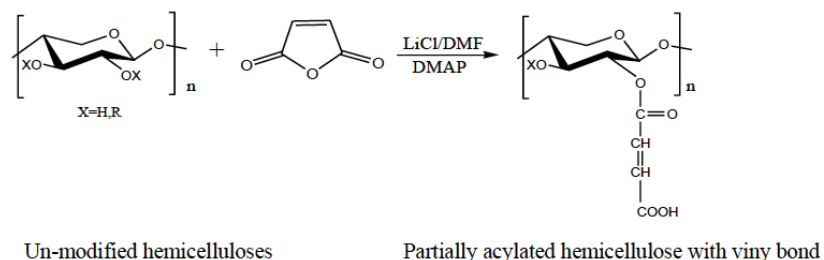
Figure 1: Partial acylation of hemicellulose.
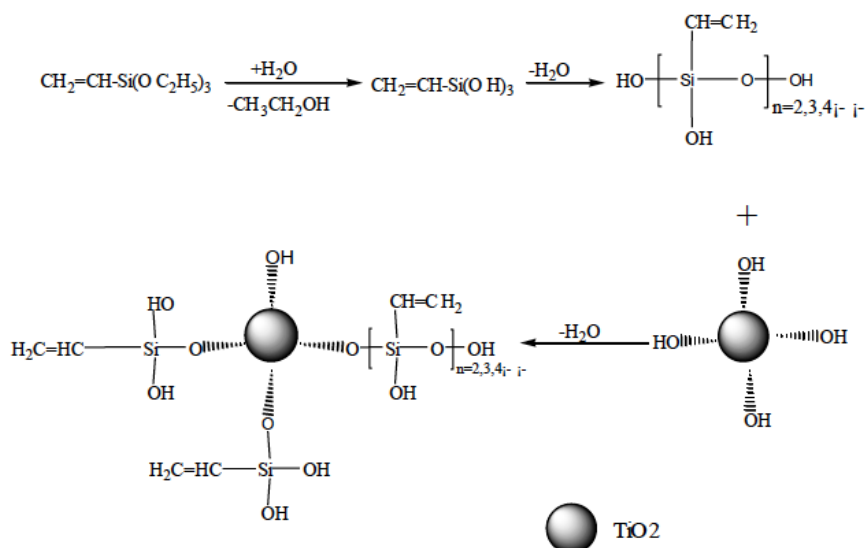
Figure 2: Modification of TiO₂ nanoparticles with silane coupling agent

The mixed solution obtained was vigorously stirred for 20 minutes and then placed in a water bath at 60 ℃ for 5 h without stirring. Upon completion of the reaction, hydrogels were taken out and cut into uniform size pieces. The samples were soaked in water for two days. During this period, it was necessary to change the water regularly for washing away the unreacted monomer. Finally, hydrogels were placed in the oven and dried to constant weight and spared.

2.5. Adsorption Studies

20 mg of hydrogels were immersed in 20 mL of methylene blue (MB) solution and swollen for 48 h at room temperature. The concentration of the remained MB solution was measured by UV-spectrophotometer at 665nm. The adsorption amount of MB, q, was evaluated according to the following equation:

$$q(mg/g) = \frac{(C_o - C_e) \times V}{1000 W_d} \tag{1}$$

where C_o (mg/L) and C_e (mg/L) are the initial concentration and the remaining concentration of MB solution, respectively; V(mL) is the volume of MB solution, and W_d (g) is the weight of dried hydrogel.

2.6. Photocatalytic Degradation Studies

Photocatalytic degradation test was carried out with a 20w UV light of wavelength λ=254nm, and the UV analyzer (ZF-6) was supplied by Shanghai Instrument Co. The photodegradation rate of MB were analyzed by testing the concentration of MB at different time, and MB self-photodegradation under UV irradiation was subtracted. The photodegradation ratio (%) was calculated using the following equation:

$$\eta = \frac{C_0 - C_t}{C_0} \times 100\% \tag{2}$$

where η is degradation ratio, C_0 is the concentration of MB solution subtracting its self-photodegradation and C_t is the concentration after photodegradation with prepared hydrogel.

3. RESULTS AND DISCUSSION

3.1. Preparation and Characterization of the Composite Hydrogel

First, hemicellulose derivative (HC-MA) has double bonds on its main chain and branch chain after being modified by maleic anhydride, and TiO₂ was modified by silane coupling agent (triethoxyvinylsilane A151) to connect double bonds on its surface. Initiating by the redox system of ammonium persulfate and anhydrous sodium sulfite, the double bonds on the modified hemicellulose and surface-modified TiO₂ were activated, and the added monomer acrylic acid was grafted onto the chain of hemicellulose and TiO₂ to form a polyacrylic chain. At the same time, the added crosslinking agent N, N-methylenebisacrylamide has two double bonds, which promoted the formation of a network structure with copolymerization and cross-linking, and TiO₂ nanoparticles were chemically cross-linked in the gel network structure. The synthesis diagram of composite hydrogel is shown in Figure **3**.

Figure **4** shows the infrared spectrum of hemicellulose, HC-MA and composite hydrogel Gel-3.
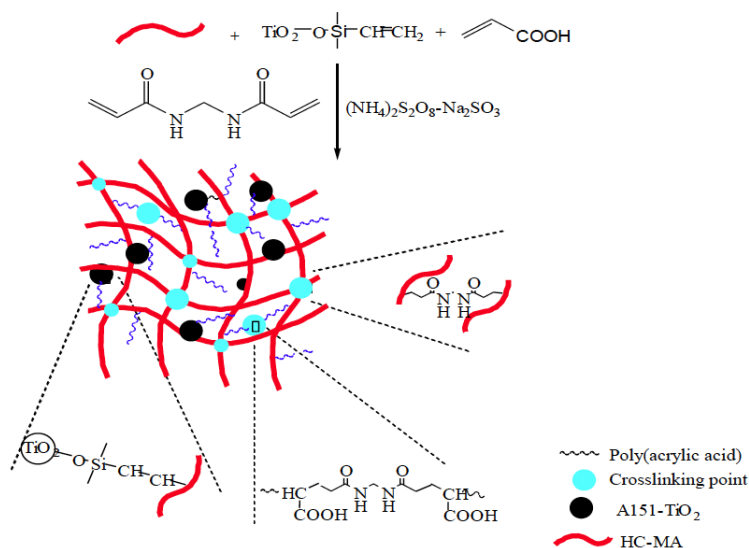
Figure 3: Schematic diagram of synthesis of the composite hydrogel.
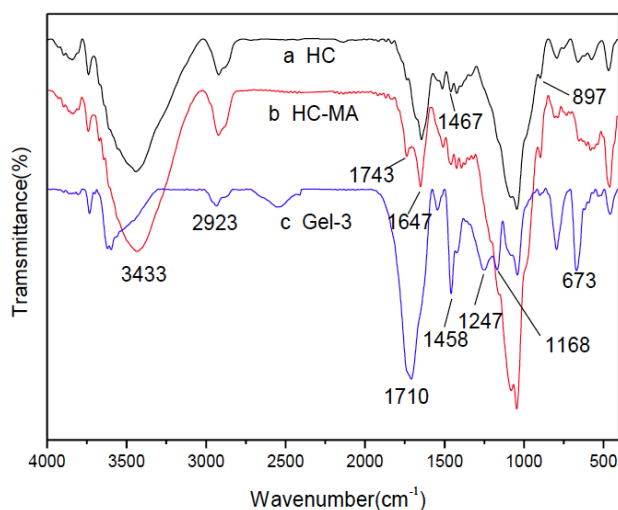
Figure 4: IR spectra of hemicellulose (a), acylated hemicellulose (b) and composite hydrogel Gel-3 (c).

It can be seen from Figure **4a** that the peaks at 3433, 2923, 1647, 1467, 1044 and 897 cm^{-1} are arisen from the absorption of hemicellulose, and the absorption peaks at 3433 and 2923 cm^{-1} are the stretching vibration peaks of O-H and C-H, respectively; The absorption peak at 1647 cm^{-1} is generated by the adsorbed water in hemicellulose, and the peak at 1044 cm^{-1} is the typical characteristic absorption of hemicellulose, which is the absorption peak of sugar unit C-O, C-O-C [15], and the characteristic absorption peak at 897cm^{-1} is generated by the frequency vibration of C1 group and ring frequency, β-Glycosidic bond between sugar units [16,17]. Compared with hemicellulose, the infrared spectrum (Figure **4b**) of HC-MA shows an obvious absorption peak at 1743cm^{-1} (C=O), indicating that hemicellulose and maleic anhydride took place esterification reaction. There is no absorption peak of maleic anhydride at 1850~1780 cm^{-1}, indicating that there is no unreacted maleic anhydride in the product; There are no carboxyl absorption peak at 1700 cm^{-1}, indicating that acid by-products were not produced during the reaction. The infrared spectrum (Figure **4c**) of Gel-3 shows the carbonyl stretching vibration absorption at 1710cm^{-1}, indicating the successful grafting of acrylic acid. The bending vibration of –C–O–H is at 1458cm^{-1}, and the asymmetric vibration band of carboxylate is at 1247 cm^{-1} and 1168cm^{-1}. The band at 673cm^{-1} is the characteristic absorption peak of TiO$_2$, indicating the existence of TiO$_2$ nanoparticles in the composite hydrogel.

Figure **5** shows the XPS spectra of A151-TiO$_2$ and hydrogel-8, and it can be seen from the figure that A151-TiO$_2$ and composite hydrogel mainly contain four
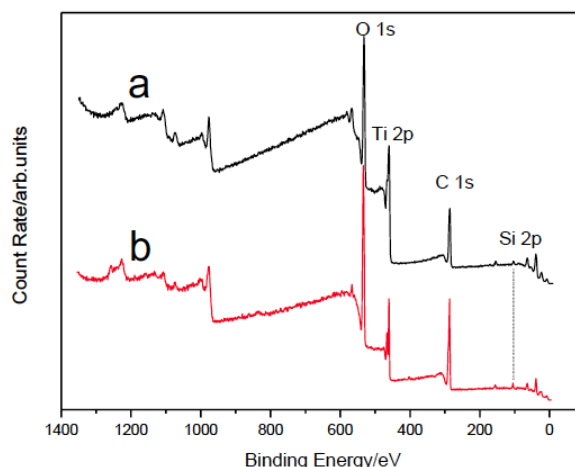
Figure 5: XPS spectra of A151-TiO$_2$ (a) and gel-8 (b)

elements: C, O, Si and Ti. The Gaussian function was used to fit the Si2p spectral line of the modified TiO_2, and the results are shown in Figure **6**, and Si mainly exists in two forms. The two peaks of binding energy Eb at 102.58 and 100.88 eV correspond to the Si-O and Si-C peaks, respectively, indicating that A151 reacts with O atoms on the TiO_2 surface, and this is because the surface of TiO_2 contains a large number of hydroxyl groups. The hydrolysis of $-Si(OC_2H_5)$ in A151 molecule produces $-Si(OH)_3$ which can dehydrate with hydroxyl groups, making A151 chemically bond to the surface of TiO_2 to form Ti-O-Si bond.
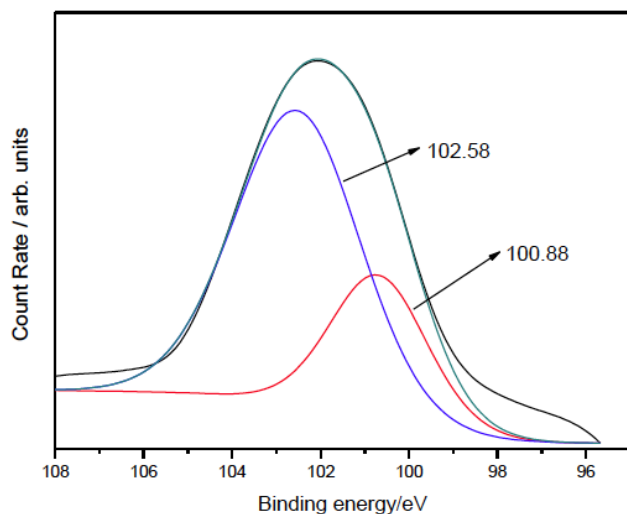
Figure 6: XPS spectrum of Si2p of modified TiO_2.

The SEM photographs of prepared composite hydrogel are shown in Figure **7**. As can be seen from Figure **7a**, the prepared hydrogel had small pore structure. Figure **7b** revealed that the pore size was around 50 μm and A151-TiO_2 nanoparticles were distributed evenly in the hydrogel. The porous structure

would be advantage for the swelling and response of the composite hydrogel.

3.2. Adsorption Study

The effect of gel dosage on MB adsorption is depicted in Figure **8a**. The MB amount adsorbed per unit mass of the gel rapidly reduced from 76.74 mg/g to 12.30 mg/g with an increase of gel dosage from 0.5 g/L to 4 g/L. The result may be because the gel had not yet reached the maximum adsorption capacity when the adsorption equilibrium reached. The pH value of the dye solution is one of the most important parameters controlling the adsorption process. Figure **8b** shows the effect of pH on adsorption amount at initial concentration of 50 mg/g. It was observed that adsorption amount increased as solution pH increased. At pH 9, the maximum adsorption amount reached, 49.49 mg/g. When pH was above 10, the adsorption amount appeared a decrease. With increasing of solution pH, the carboxyl groups were hydrolyzed to $-COO^-$, which provided the impetus for combination of adsorbent and MB. However, the concentration of cationic Na^+ also increased when pH increased, which had side effects on swelling and adsorption of ionic hydrogel. Therefore, adsorption capacity decreased at higher pH.

Effect of initial concentration on adsorption amount is displayed in Figure **8c**. It appeared that adsorption amount increased from 46.65 mg/g to 292.24 mg/g with an increase of MB concentration from 50 mg/L to 400 mg/L. The higher MB concentration provided a higher driving force for MB molecules onto the adsorbent, so the adsorption amount of MB enhanced. Figure **8d** shows the variation of adsorption amount with
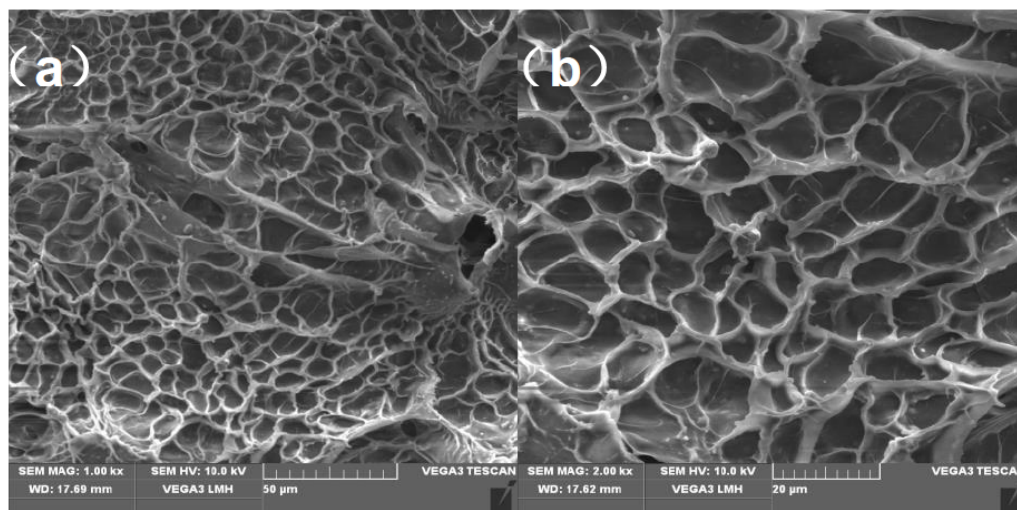
Figure 7: SEM photographs of prepared gel: (**a**) ×10,000; (**b**) ×20,000.
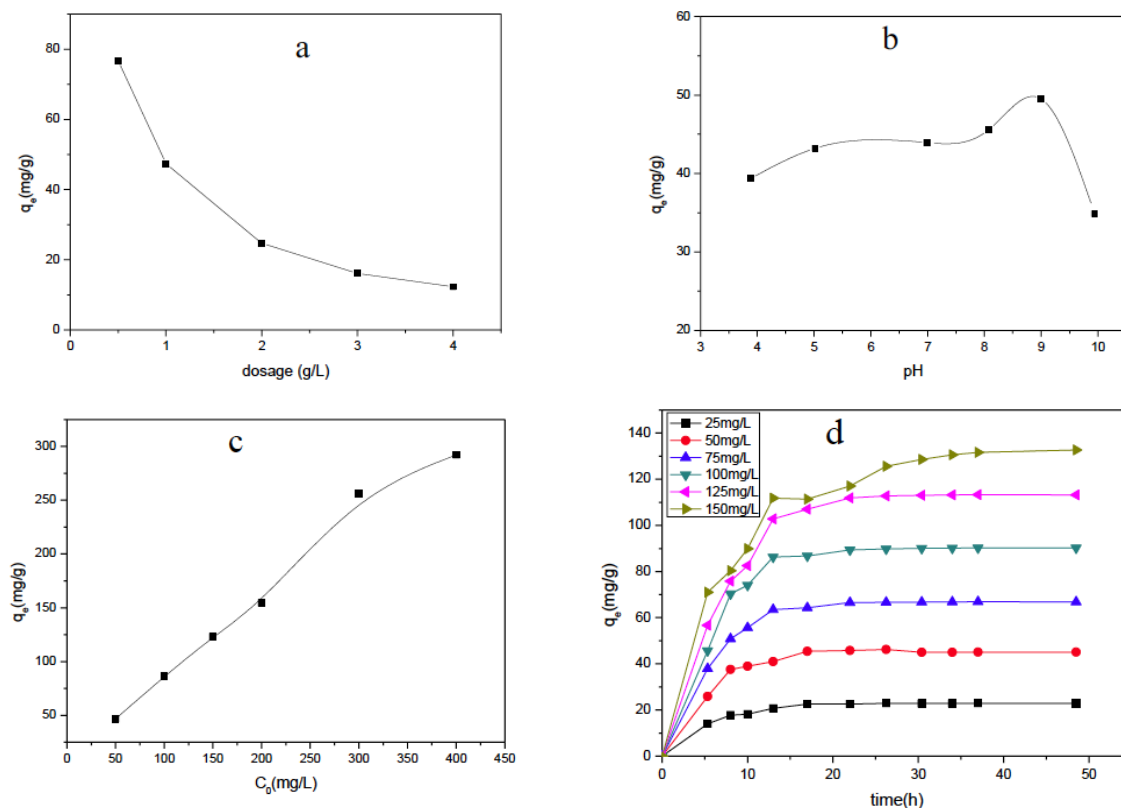
Figure 8: Effects of adsorption conditions on adsorption capacity of the prepared hydrogel (**a**, gel dosage; **b**, pH; **c**, initial concentration of MB solution; **d**, contact time).

increased contact time. A high adsorption rate appeared at the initial adsorption period followed by a much slow rate, and the adsorption ultimately achieved a balance. The phenomenon can be explained by the fact that the adsorption sites of the hydrogel and the dye molecules had interacted within the first few minutes and the continuous adsorption for the dye only appeared in its internal adsorption sites, leading to a slow growth rate of adsorption amount.

Adsorption isotherm study can find how adsorbate molecules interact with adsorbent surface. The Freundlich and Langmuir models are used to study the adsorption isotherm. Freundlich equation is described as equation 3 [18]:

$$\log q_e = \log K_F + \frac{1}{n}\log C_e \tag{3}$$

Langmuir equation is shown as equation 4 [18].

$$\frac{C_e}{q_e} = \frac{C_e}{q_{max}} + \frac{1}{K_L q_{max}} \tag{4}$$

where q_e is equilibrium adsorption capacity of absorbent; C_e is the remaining MB concentration at adsorption equilibrium; K_F and K_L are the constant of

Freundlich equation and Langmuir equation, respectively; n represents indicator of adsorption intensity; q_{max} is the maximum adsorption capacity of absorbent at monolayer coverage.

Freundlich isotherm and Langmuir isotherm graphs acquired by experimental data are shown in Figure **9a** and **9b**, respectively. The calculated parameters and correlation coefficient (R^2) are summarized in Table **1**. It is evident that the Freundlich model is better to describe the adsorption of MB onto the absorbent than Langmuir model, suggesting the heterogeneous surface adsorption of methylene blue. The prepared composite hydrogel possessed a porous structure, which provided the path for dye diffusion into absorbent.

To investigate the adsorption process, four adsorption kinetic models were applied to analyze the obtained experimental data: the pseudo-first-order [19], the pseudo-second-order [20], the Elovich equation [21] and the intra-particle diffusion models [22].

The pseudo-first-order kinetic equation:

$$\log(q_e - q_t) = \log q_e - \frac{k_1}{2.303}t \tag{5}$$
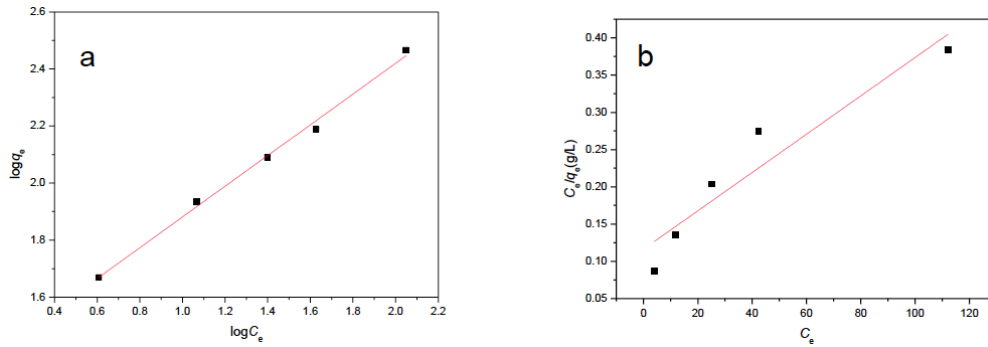
Figure 9: Freundlich (**a**) and Langmuir (**b**) isotherm graphs for adsorption of MB at room temperature.

Table 1:   Freundlich and Langmuir Isotherm Coefficients for MB

Freundlich parameters			Langmuir parameters		
1/n	K_F	R^2	q_{max}	K_L	R^2
0.53915	21.96945	0.9939	389.1051	0.022058	0.87702

The pseudo-second-order kinetic equation:

$$\frac{t}{q_t} = \frac{1}{k_2 q_e^2} + \frac{1}{q_e} t \qquad (6)$$

Elovich equation:

$$q_t = \frac{1}{b}\ln(ab) + \frac{1}{b}\ln t \qquad (7)$$

Intra-particle diffusion kinetic equation:

$$q_t = K_p t^{1/2} + C \qquad (8)$$

where q_e is the adsorbed dye amount per unit mass of adsorbent at equilibrium (mg/g), and q_t represents the adsorption amount of MB at time t (h); t is the adsorption time (h), and k_1, k_2, a and K_p are the rate constants of the corresponding model.
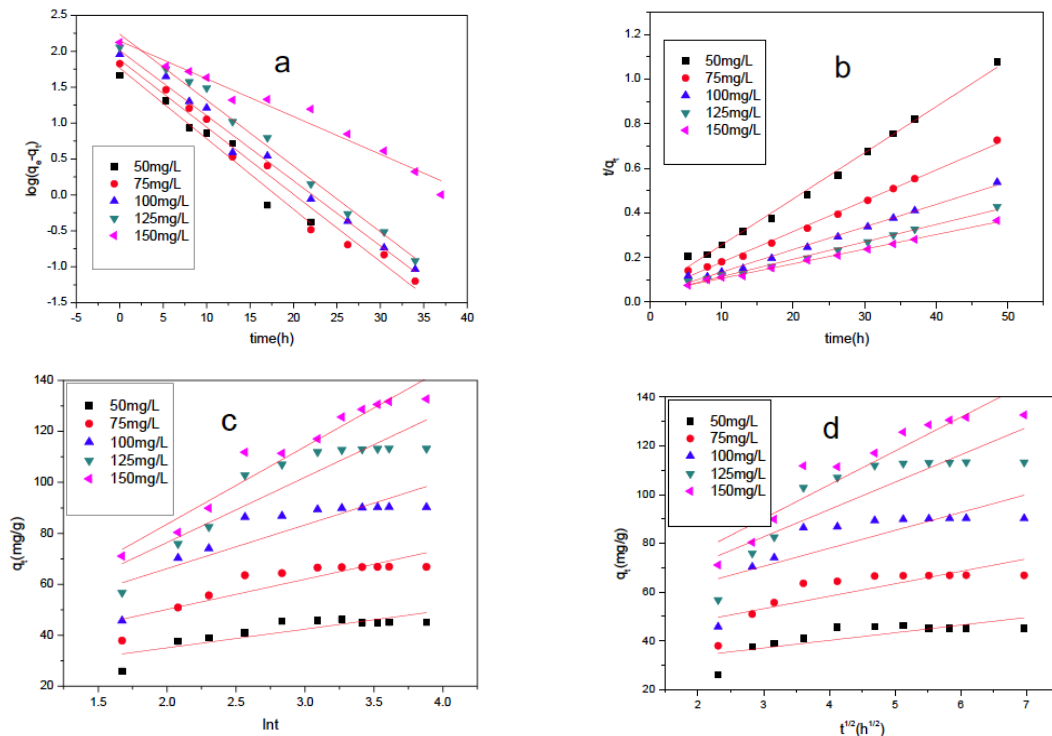
Figure 10: Four adsorption kinetic models for adsorption of MB (a, the pseudo-first-order kinetic model; b, the pseudo-second-order kinetic model; c, Elovich equation; d, Intra-particle diffusion kinetic model).

Table 2: Kinetic Parameters of Four Models for MB onto Adsorbent

Kinetics	Parameters	MB concentrations (mg/L)				
		50	75	100	125	150
Pseudo-first-order	q_e^a, mg/g	45.0823	66.8734	90.2562	113.3144	132.6863
	K_1, h^{-1}	0.226224	0.215561	0.208767	0.211208	0.121092
	q_e^b, mg/g	58.22239	75.8472	102.221	172.2463	138.7714
	R^2	0.9511	0.9789	0.9884	0.9888	0.9678
Pseudo-second-order	q_e^b, mg/g	48.3092	72.4113	98.7167	128.2051	152.4390
	K_2, g/(mg.h)	0.008757	0.004742	0.00309	0.001687	0.001063
	R^2	0.9936	0.9949	0.9914	0.9905	0.9964
Elovich equation	a	118.1271	110.9376	110.6336	68.7879	64.3967
	b	0.1362	0.0845	0.0584	0.0391	0.0329
	R^2	0.6863	0.7599	0.7169	0.8275	0.9404
Intraparticle-diffusion	K_p	3.1356	5.1180	7.3609	11.2254	13.8530
	C	27.5852	37.7802	48.4888	48.9614	48.6149
	R^2	0.5398	0.6180	0.5739	0.6985	0.8665

Figure **10** shows the four adsorption kinetic models for MB adsorption on the prepared adsorbent. The obtained adsorption kinetics factors are given in Table **2**, which were obtained by calculating obtained experimental data. It was clear that the pseudo-second order equation was the best model to explain the adsorption of MB on the prepared hydrogels by comparing the linear correlation coefficient R^2. This model can describe the whole adsorption process including the adsorption of MB on the surface of the hydrogels, the diffusion of MB from the surface of the hydrogels into the active sites and the final adsorption process.

3.3. Photocatalytic Degradation

Figure **11a** depicts the effect of the initial concentration of MB solution on photodegradation. As shown in Figure **11a**, when the initial concentration of MB solution increased from 50mg/L to 150mg/L, the photodegradation rate of MB increased from 59% to 85% as a result of an increase in the MB adsorption amount of absorbent. The effect of initial pH of MB solution was also shown in Fig. 11b, and the photocatalytic efficiency of the adsorbent were higher under alkaline conditions than that under acidic conditions, and the photocatalytic activities enhanced along with alkalinity increase of MB solution. The composite gel exhibited the highest photodegradation ratio of over 90% at pH=10. These phenomena were possible due to the fact that excess of OH$^-$ anions facilitated photogeneration of hydroxyl radicals, which enhanced the rate of degradation [23, 24].

CONCLUSIONS

A hemicellulose-*g*-PAAc/TiO$_2$ composite hydrogel was prepared and used to remove MB from aqueous solution. The obtained results showed that the equilibrium adsorption data fitted well to the Freundlich
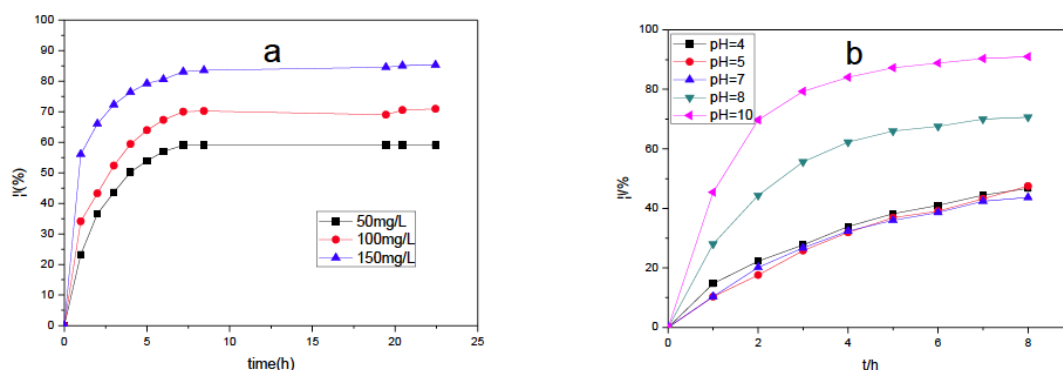
Figure 11: Effects of initial concentration and pH on photodegradation rate (a, initial concentration; b, pH).

isotherm, and the pseudo second-order kinetic model was suitable to describe the adsorption process. Effects of adsorbent dosage, pH, initial concentration and contact time on the adsorption and photodegradation of the prepared adsorbent were studied to apprehend a comprehensive understanding of the prepared photocatalyst. The prepared composite hydrogel exhibited high photodegradation ability for MB under alkaline conditions, and the maximum photodegradation percent can reach over 90%. Meanwhile, increasing initial concentration and contact time further enhanced the removal efficiency of MB.

DECLARATION OF COMPETING INTEREST

The authors declare no conflict of interest.

ACKNOWLEDGEMENTS

CREDIT AUTHOR STATEMENT

Xiao-Feng Sun Writing-original draft, Writing-review and editing, Conceptualization, and Funding acquisition; Yudan Li and Jiayi Chen Investigation and Methodology; Jiayi Chen and Le Sun, Visualization, Formal analysis and Validation. All authors have read and agreed to the published version of the manuscript.

REFERENCES

[1]   Tanaka K, Padermpole K, Hisanaga T. Photocatalytic degradation of commercial azo dyes. Water Research 2000; 34: 327-333.
https://doi.org/10.1016/S0043-1354(99)00093-7

[2]   Sun XF, Sun RC, Fowler P, Baird MS. Extraction and characterization of original lignin and hemicelluloses from wheat straw. J Agr Food Chem 2005; 53: 860-870.
https://doi.org/10.1021/jf040456q

[3]   Sun XF, Zeng QH, Wang HH, Hao Y. Preparation and swelling behavior of pH/temperature responsive semi-IPN hydrogel based on carboxymethyl xylan and poly(N-isopropyl acrylamide). Cellulose 2019; 26: 1909-1922.
https://doi.org/10.1007/s10570-018-2180-x

[4]   Sun XF, Gan Z, Jing ZX, Wang HH, Wang D, Jin YN. Adsorption of methylene blue on hemicellulose-based stimuli-responsive porous hydrogel. Journal of Applied Polymers Science 2015; 132.
https://doi.org/10.1002/app.41606

[5]   Barbat A, Gloaguen V, Moine C, Sainte-Catherine O, Kraemer M, Rogniaux H, Ropartz D, Krausz P. Structural characterization and cytotoxic properties of a 4-O-methylglucuronoxylan from castanea sativa. 2. Evidence of a structure−activity relationship. J Nat Prod 2008; 71: 1404-1409.
https://doi.org/10.1021/np800207g

[6]   Söderqvist-Lindblad M, Albertsson AC, Ranucci E, Laus M, Giani E. Biodegradable polymers from renewable sources: rheological characterization of hemicellulose-based hydrogels. Biomacromolecules 2005; 6: 684-690.
https://doi.org/10.1021/bm049515z

[7]   Coviello T, Matricardi P, Marianecci C, Alhaique F. Polysaccharide hydrogels for modified release formulations. J Control Release 2007; 119: 5-24.
https://doi.org/10.1016/j.jconrel.2007.01.004

[8]   Lee WF, Chen YC. Effects of intercalated hydrotalcite on drug release behavior for poly(acrylic acid-co-N-isopropyl acrylamide)/intercalated hydrotalcite hydrogels. European Polymer Journal 2006; 42: 1634-1642.
https://doi.org/10.1016/j.eurpolymj.2006.01.014

[9]   Wang C, Flynn NT, Langer R. Controlled structure and properties of thermoresponsive nanoparticle-hydrogel composites. Advanced Materials 2004; 16: 1074-1079.
https://doi.org/10.1002/adma.200306516

[10]   Xiang Y, Chen D. Preparation of a novel pH-responsive silver nanoparticle/poly(HEMA-PEGMA-MAA) composite hydrogel. European Polymer Journal 2007; 43: 4178-4187.
https://doi.org/10.1016/j.eurpolymj.2007.08.005

[11]   Dalaran M, Emik S, Güçlü G, İyim TB, Özgümüş S. Study on a novel polyampholyte nanocomposite superabsorbent hydrogels: Synthesis, characterization and investigation of removal of indigo carmine from aqueous solution. Desalination 2011; 279: 170-182.
https://doi.org/10.1016/j.desal.2011.06.004

[12]   Lee WF, Fu YT. Effect of montmorillonite on the swelling behavior and drug-release behavior of nanocomposite hydrogels. J Appl Polym Sci 2003; 89: 3652-3660.
https://doi.org/10.1002/app.12624

[13]   Shirsath SR, Hage AP, Zhou M, Sonawane SH, Ashokkumar M. Ultrasound assisted preparation of nanoclay Bentonite-FeCo nanocomposite hybrid hydrogel: A potential responsive sorbent for removal of organic pollutant from water. Desalination 2011; 281: 429-437.
https://doi.org/10.1016/j.desal.2011.08.031

[14]   Dong W, Huang C, Wang Y, Sun Y, Ma P, Chen M. Superior Mechanical Properties of Double-Network Hydrogels Reinforced by Carbon Nanotubes without Organic Modification. Int J Mol Sci 2013; 14: 22380-22394.
https://doi.org/10.3390/ijms141122380

[15]   Sun XF, Ye Q, Jing ZX, Li YJ. Preparation of hemicellulose-g-poly(methacrylic acid)/carbon nanotube composite hydrogel and adsorption properties. Polym Composite 2014; 35: 45-52.
https://doi.org/10.1002/pc.22632

[16]   Li YJ, Sun XF, Ye Q, Liu BC, Wu YG. Preparation and property of novel hemicellulose-based magnetic hydrogel. Acta Physico-Chimica Sinica 2013; 35: 111-120.
https://doi.org/10.3866/PKU.WHXB201310313

[17]   Sun XF, Xie Y, Shan S, Li W, Sun L. Chemically-crosslinked xylan/graphene oxide composite hydrogel for copper ions removal. J Polym Environ 2022; 30: 3999-4013.
https://doi.org/10.1007/s10924-022-02475-5

[18]   Langmuir I. The adsorption of gases on plane surfaces of glass, mica and platinum. Journal of the American Chemical Society 1918; 40: 1361-1403.

[19]   Langergren S, Svenska K. About the theory of so-called adsorption of soluble substances. Vetenskapsakademiens Handlingar 1898; 24: 1-39.

[20]   Ho YS, McKay G. Pseudo-second order model for sorption processes. Process Biochemistry 1999; 34: 451- 465.
https://doi.org/10.1016/S0032-9592(98)00112-5

[21]   Aharoni C, Tompkins FC. Kinetics of adsorption and desorption and the Elovich equation, In: Eley DD, Pines H, Weisz PB, (Eds.). Advances in Catalysis, Academic Press, New York 1970; 21: 1-49.
https://doi.org/10.1016/S0360-0564(08)60563-5

[22]   Weber WJ, Morris JC. Kinetics of adsorption on carbon from solution. J Sanit Eng Div 1963; 89: 31-59.
https://doi.org/10.1061/JSEDAI.0000430

[23]   Xie Y, Sun XF, Li W, He J, Sun R, Hu S, Wu Y. Fabrication of electrospun xylan-g-pmma/TiO_2 nanofibers and

photocatalytic degradation of methylene blue. Polymers 2022; 14: 2489.
https://doi.org/10.3390/polym14122489

[24]   Böttcher H, Mahltig B, Sarsour J, Stegmaier T. Qualitative investigations of the photocatalytic dye destruction by TiO2-coated polyester fabrics. Journal of Sol-gel Science and Technology 2010; 55: 177-185.
https://doi.org/10.1007/s10971-010-2230-9